Investigation of the hydro-mechanical behaviour of a pellet/powder MX80 bentonite mixture using an infiltration column

Agustín Molinero Guerra, Yu-Jun Cui, Nadia Mokni, Pierre Delage, Michel Bornert, Patrick Aimedieu, Anh Minh A.M. Tang, Frédéric Bernier

Investigation of the hydro-mechanical behaviour of a pellet/powder MX80 bentonite mixture using an infiltration column

Agustín Molinero Guerra[1,2], Yu-Jun Cui[1*], Nadia Mokni[2], Pierre Delage[1], Michel Bornert[1], Patrick Aimedieu[3], Anh Minh Tang[1], Frédéric Bernier[4]

[1]Ecole des Ponts ParisTech, Laboratoire Navier/CERMES, Marne La Vallée, France
[2]Institut de Radioprotection et de Sûreté Nucléaire (IRSN), Fontenay-aux-Roses, France
[3]Laboratoire Navier, UMR 8205, ENPC, IFSTTAR, CNRS, UPE, Champs-sur-Marne 77455, France
[4]Agence Fédérale de Contrôle Nucléaire (AFCN), Belgium

*Corresponding author

Prof. Yujun Cui
Ecole des Ponts ParisTech
6-8 av. Blaise Pascal
Cité Descartes, Champs-sur-Marne
77455 Marne la Vallée
France

E-mail: yu-jun.cui@enpc.fr

Abstract:

Non-compacted pellet/powder bentonite mixtures are considered as candidate sealing plug materials in geological disposals of radioactive waste. Due to its nature, this mixture is characterized by a heterogeneous porosity network, which is responsible for its complex hydro-mechanical (HM) behaviour. The French Institute of Radioprotection and Nuclear Safety (IRSN) has investigated this mixture within the SEALEX project. Both *in situ* large-scale and laboratory small-scale experiments were carried out. This paper presents the results of a small-scale mock-up test at $1/10^{th}$ scale of the *in situ* experiments, in which the pellet/powder mixture was saturated from both sides (top and bottom of the specimen). Both swelling pressure and relative humidity were monitored at several positions of the specimen. Different responses from the sensors were found, depending on the local porosity as well as the evolution of the hydration front. The HM response of the mixture is strongly conditioned by the initial pellet/powder distribution, which depends on the protocol followed for the specimen preparation. After 800-day hydration, an anisotropy was found between the axial and the radial swelling pressures, due to the presence of larger void at the top of the sample and the friction at the cell wall. The sample was still heterogeneous after 800-day hydration mainly due to the initial heterogeneous porosity distribution, combined with the effect of friction and the non-saturation of the mixture. The evolution of injected water with time revealed that the sample was not full saturated after 800-day hydration.

Keywords: pellet/powder bentonite mixture; heterogeneous porosity network; mock-up test; swelling pressure; relative humidity

1. Introduction

Powder/pellet bentonite mixtures are considered as one of the candidate sealing materials for deep underground radioactive waste repositories thanks to their favourable properties: high swelling capacity, high radionuclide migration retardation properties and operational advantages: easy to manufacture and install (especially in vertical shafts). Once installed in the gallery, the pellet/powder bentonite mixture is initially unsaturated. Then, the saturation process starts under constrained volume condition due to the infiltration of pore water from the host rock, generating a swelling potential that allows filling the voids within the mixture. Due to its nature, these mixtures are characterized by an initial heterogeneous porosity distribution (Molinero Guerra et al., 2016), which results in a complex hydro-mechanical behaviour during the saturation process. It is therefore essential to investigate this swelling behaviour in order to validate the material for the sealing plug in the underground radioactive waste disposal.

In this context, the Institute of Radioprotection and Nuclear Safety (IRSN, France) has launched the SEALEX (SEALing performance Experiments) project, within which the work presented here was conducted. The purpose of this project is to investigate the long-term hydraulic performance of sealing systems in normal and critical scenarios, as well as different core compositions and configurations (mixture composed of bentonite pellets with bentonite powder or of sand with bentonite powder, pre-compacted or *in situ* compacted). Figure 1 presents the layout of the experiments.

The hydro-mechanical behaviour of different configurations of sealing plugs was investigated at both laboratory and field scales (Wang et al., 2012; Saba et al., 2014; Mokni et al., 2016). An important result from these investigations is the relationship between the swelling pressure and the dry density of bentonite (Börgesson et al., 1996; Dixon et al., 1996; Lloret et al., 2003; Karnland et al., 2008; Gens et al., 2011; Villar et al., 2012 ; Wang et al., 2013; Saba et al., 2014;

Schanz & Al-Badran, 2014). These relationships were derived on the basis of the measured axial swelling pressure of the investigated materials. However, few investigations have been carried out on the radial swelling of the studied sealing plug (Saba et al., 2014). Therefore, it is fundamental to further investigate the complex patterns governing the swelling behaviour of the initially heterogeneous mixture of pellet/powder of bentonite in order to ensure that this repository configuration design meets the performance targets.

The swelling capacity of pellet/powder bentonite mixtures was investigated by Imbert & Villar (2006) through a series of infiltration tests on a 50/50 pellet/powder FoCa bentonite compacted at different dry densities. After full saturation, the swelling pressure was found analogous to that of a specimen of powder compacted at the same dry density. Van Geet et al. (2005) studied the hydration process of a 50/50 pellet/powder FoCa bentonite mixture by X-ray computed tomography. The results showed the progressive decrease of the density of pellets and the apparent homogenisation after saturation. Other sealing plug configurations were investigated by mock-up tests. Wang et al. (2013) and Saba et al. (2014) studied a compacted MX80 bentonite/sand mixture (with a proportion of 70/30 in dry mass). Saba et al. (2014) investigated the anisotropy of swelling pressure of compacted bentonite/sand mixture. μCT observations revealed that the material was looser in the radial direction than in the axial one. The homogenisation process of a granular material made of highly compacted bentonite pellets (granular buffer material, GBM) was investigated by Garcia-Siñeriz et al. (2015) under the context of the EB (engineered barrier) experiment. Upon dismantling, a gradient of density and water content was found within the GBM, probably due to the initial heterogeneity of the material (Villar, 2013).

No investigations have been carried out on the swelling of non-compacted pellet/powder bentonite mixtures. This is however crucial in the design of sealing plugs for deep radioactive waste disposal, because the initial heterogeneous distribution of porosity of these configurations

might result in an anisotropy of swelling. Therefore, this study aims at investigating the HM behaviour of this kind of mixture by simulating the SEALEX *in situ* experiments at a small scale ($1/10^{th}$, resulting in 60 mm in diameter and 120 mm in height). Radial swelling pressure at different positions, as well as axial swelling pressure and relative humidity were monitored during hydration from both sides (top and bottom of the sample). The volume of injected water was also recorded during the test.

2. Investigated material

The soil studied is a mixture of pellet/powder MX80 bentonite at a proportion of 80/20 in dry mass. The bentonite investigated comes from Wyoming, USA. It was provided by the Laviosa-MPC company under the commercial name Expangel SP7 for pellets and SP30 for the powder. The MX80 bentonite has a smectite content of 80%, other minerals being quartz, calcite and pyrite. The cation exchange capacity (CEC) is 98 meq/100g, with Na+ as major exchangeable cation (52 meq/100g). The liquid limit is 560%, the plastic limit is 62% and the unit mass is 2.77 Mg/m^3 (Saba et al., 2014).

Pellets of bentonite were produced by Laviosa-MPC Company by compaction of a powder of MX80 bentonite in a mould of 7 mm in diameter and 7 mm in height. Compaction was performed at a water content of 6±1% by applying instantaneous compaction effort by following the vertical axis of the pellet, resulting in a pellet dry density ρ_d = 2.06±0.06 Mg/m^3, corresponding to a void ratio e = 0.30±0.07. The pellets were stored in the laboratory in a hermetic plastic box at 20°C. The initial suction (s = 135 ± 3 MPa) was measured in the laboratory with a chilled mirror dew point tensiometer (Decagon WP4C), at an initial water content w = 7.25%, slightly higher than the fabrication one, due to further hydration after fabrication (Molinero Guerra et al., 2016).

128 The MX80 bentonite powder was produced by crushing pellets. An initial water content of
129 3.17% was found in the laboratory after drying at 105°C for 24 h, corresponding to an initial
130 suction s = 190.9 MPa (measured with a chilled mirror dew point tensiometer – Decagon WP4).
131 More details about the initial state of the material can be found in Molinero Guerra et al. (2016).

132 The saturation water used in the test is synthetic water having the same chemical composition
133 as the pore water of the Callovo-Oxfordian claystone from the ANDRA underground research
134 laboratory in Bure (

Table 1). The water was obtained by mixing the chemical components with distilled water until full dissolution.

Results of mercury intrusion porosimetry (MIP) tests for a pellet of bentonite at its initial state are presented in Figure 2. A pore population with an average entrance diameter of 11.9 nm is detected, as well as a second one at diameters around 4 – 5 μm that represents 6.8% of the total porosity. For the pellet/powder mixture, macro-voids existing between pellets and powder grains will play an important role in the HM behaviour. The investigated material is characterized by a multimodal porosity network with a heterogeneous distribution of the porosity within the sample. The latter was demonstrated by a qualitative analysis of a vertical slice obtained by carrying out μ-CT observations of a pellet/powder bentonite mixture prepared by following the same protocol as the investigated specimen in the mock-up test (Figure 3). This feature is crucial since it conditions the overall HM behaviour of the material.

3. Experimental methods

3.1. Experimental set-up

The layout of the small-scale infiltration cell (mock-up test cell) is presented in Figure 4. The dimensions correspond to $1/10^{th}$ of the *in situ* SEALEX experiments (60 mm in diameter and 120 mm in height). The confined saturation conditions for the pellet/powder bentonite mixture are ensured by a rigid structure that keeps a zero radial displacement (the estimated axial strain is 5×10^{-6}) and a piston blocked by a screw, which prevents any axial displacement. The material is saturated from both sides (top and bottom), simulating the SEALEX *in situ* experiments. The sample is placed between two pore stones and two filter papers. The bottom and the upper bases are equipped with a water inlet and an air outlet. The air outlet is needed to evacuate the air that is present in the base and in all the system near the inlets. Mechanical valves are mounted and sealed at the faces of both inlets, allowing the entrance of water and

159 the evacuation of air. Flexible water hoses are connected to the valves. The side serving as a
160 water inlet is connected to a burette and to a water tank, allowing the volume of injected water
161 to be measured during hydration. Six total pressure sensors are installed in the cell (SP20, SP40,
162 SP60, SP80, SP100 and SP120), which allow the measurements of the radial swelling pressures
163 at different positions (h = 20, 40, 60, 80, 100 and 120 mm from the bottom side). Figure 3
164 presents the pellet/powder mixture together with the position of the radial swelling pressure
165 sensors. A force transducer is installed under the cell base, which monitors the axial swelling
166 pressure. In this study, the relative humidity is also recorded by five relative humidity sensors
167 (RH31, RH51, RH71, RH91 and RH111) placed at different heights (h = 31, 51, 71, 91 and 111
168 mm, see Figure 4), allowing the evolution of suction to be monitored while hydration.

169 ### 3.2. Sample preparation and test procedure

170 The sample was prepared directly into the cell that was already placed on the tray of the force
171 transducer with the radial sensors screwed to the cell. The pellet/powder mixture was obtained
172 by following the first protocol proposed in Molinero Guerra et al. (2016), which allows a
173 relatively homogeneous sample to be obtained. However, a perfect homogeneous distribution
174 cannot be obtained due to the nature of the mixture. It was to fill the cell by packets
175 corresponding to one layer of pellets spread over the base of the cylinder and to add the
176 corresponding amount of powder (taking into account the proportion 80% pellets – 20% powder
177 in dry mass). Figure 3 presents a vertical section of the pellet/powder mixture obtained by
178 microfocus X-ray computed tomography observations on a sample at its initial state, together
179 with the positions of the swelling pressure sensors. The global dry density is 1.49 Mg/m^3.

180 Once the sample was prepared, the two stainless steel plates were fixed with three rods. The
181 central screw was adjusted to ensure the constant volume conditions. The test was started by
182 opening the water inlet valves. At the beginning of the test, air in the base or in the piston was
183 evacuated by opening the air outlet valve until no air bubble was observed in the pipes.

Synthetic water was injected by both the top and the bottom of the sample, as the SEALEX *in situ* experiments. The applied water pressure while hydration was equal to the atmospheric pressure at both top and bottom boundaries. Radial and axial swelling pressures, as well as relative humidity were recorded automatically by a data logger. The volume of injected water was also controlled while hydration by two graduated burettes connected to the hydration system. No water pressure was applied during the saturation process.

4. Results

4.1. Investigation of the swelling pressure

The evolution of the swelling pressure with a zoom on the first 15 days is shown in Figure 5. A different rate of increase is identified for each sensor. For sensor SP100, located at 100 mm from the bottom (and 12 mm from the top hydration front), an initial fast increase of swelling pressure is observed, reaching a peak value of 2.15 MPa, then a decrease until 1.5 MPa, and finally an increase to reach stabilisation at about 2.5 MPa. This phenomenon occurs during the first hours of hydration. For other sensors, the rates of increase are similar, being the sensor located at 20 mm from the bottom (SP20) the one who exhibits a higher swelling pressure after 15 days (1.5 MPa), because of its proximity to the front of hydration. The difference in the increase rate depends on the evolution of the hydration front as well as the local porosity of the material characterized by an initial heterogeneous distribution of macro-porosity. After a few hours, water reaches sensor SP40. This sensor presents a negative rate at the beginning of the test, which could be interpreted as a collapse of the material at this level due to the presence of larger voids. The evolution of SP60 indicates that water arrives after 4 days of hydration.

Figure 6 presents the evolution of swelling pressure during 200-day hydration. The lowest swelling pressure and increase rate are observed for sensor SP120, located at the top of the sample. This is because, at this level, the sensor is in contact with the porous stone (see Figure

3), thus the response does not correspond to the behaviour of the soil. For the sensors located at the middle position (SP40, SP60, SP80 and SP100), the increase rate and the swelling pressure depend not only on the distance to the hydration front, but also on the local porosity defined by the pellets/powder grains distribution. A common value of about 2.5 MPa of swelling pressure is reached after 60 days of hydration except for SP20. Afterwards, sensors SP40, SP60 and SP80 exhibit the same increase rate until 110 days of hydration, where a stabilized swelling pressure is reached. At 120 days, SP80 presents an increase of swelling pressure followed by a stabilization at 135 days of hydration. Sensor SP100 presents a different response: an increase of swelling pressure is observed after 60 days, with a value almost constant, and then at 93 days it increases again to reach a constant value (the same increase is observed for SP40, SP60 and SP80), lower than the swelling pressures from other radial sensors (except that at 120 mm, which value is the lowest as it was explained previously). It should be noted that the swelling pressures after 200 days are different for all the sensors. This phenomenon will be discussed later. The axial swelling pressure corresponds to the global pressure transmitted to the piston, and its value is lower than those from other sensors. However, no consistent comparison can be made with the radial rates since in the latter case the pressures are measured locally. The rate of increase of the axial swelling pressure cannot be compared to the radial rates as the force transducer measures a global force and not the local total pressure.

According to the cell design (Figure 4), the swelling pressure of the material is transmitted to the upper piston, and then the force is transmitted to the force transducer. Therefore, two phenomena should be considered to interpret the measured axial swelling pressure: (i) the local porosity at the top of the sample, which is higher due to the presence of larger voids (see Figure 3, where the porous stone is in contact with some pellets at the top of the sample but there is no powder at this level) and (ii) the effect of friction. These two combined phenomena might explain the lower value of swelling pressure.

233 The evolution of the swelling pressures for 845-day hydration is shown in Figure 7. Some
234 oscillations are observed after 200 days of hydration. These oscillations could be due to
235 laboratory temperature changes. They are not related to electrical problems because the
236 response of the sensors was corrected with respect to the electrical voltage. After 700 days of
237 hydration, a common value of about 4 MPa of swelling pressure is reached for sensors SP20,
238 SP40, SP60 and SP80. Sensor SP100 still remains at a lower value, slightly higher than 3 MPa,
239 as well as the axial pressure (2.5 MPa).

240 Figure 8 presents the swelling pressure profiles at a time interval of 5 days. As it was explained
241 before, the swelling pressure at 120 mm is not representative because the sensor is in contact
242 with the porous stone at this level. At the bottom of the sample, the increasing rate of swelling
243 pressure is lower because there might not be preferential arrangement of pellets at this level.
244 After 50 days of hydration, the lowest value of swelling pressure is at 60 mm, which
245 corresponds to the farthest position from the hydration front. These heterogeneous swelling
246 pressure values depend on the local porosity of the material, which is controlled by the initial
247 pellet/powder distribution within the sample. The profiles of swelling pressure every 100 days
248 are shown in Figure 9. An increase of the swelling pressure is observed at 40 mm, 60 mm and
249 80 mm due to the evolution of the hydration front and the consequent swelling of the material
250 at these levels. A heterogeneity of the final value of swelling pressure is observed after 800
251 days of hydration, with a mean value slightly higher than 4 MPa.

252 ### 4.2. Investigation of the relative humidity

253 The evolution of the relative humidity with time is shown in Figure 10. Starting at 36.7%
254 relative humidity corresponding to 138 MPa of suction, the curves show different rates for
255 different sensors. Those located close to the front of hydration (RH31 and RH111) exhibit the
256 highest rates, and a value of 100% is reached after 15 days for RH111 and 20 days for RH31.
257 Sensor RH111, located at 9 mm from the top hydration front, exhibits the highest rate because

of the effect of gravity and the presence of voids at this level of the sample (Figure 3), which creates preferential paths for injected water. For sensors RH51 and RH91 the increase rate is similar, and saturation is reached after 45 days of hydration. Sensor RH71, located at 29 mm from the top hydration front, exhibits the lowest increase rate, with a value of 100% reached after almost 50-day hydration. The response of the sensors located at an intermediate position in the sample (RH51, RH71 and RH91) depends on the evolution of the hydration front.

The total volume of water injected while hydration, as well as the volume injected by the top and the bottom are presented in Figure 11. At the beginning of the test, the rate of increase is comparable for the top and bottom injection. However, a higher volume is injected by the top due to the existence of larger voids (Figure 3) combined with the gravity effect. The infiltration by the top of the specimen is controlled by the water level of the burette which hydrates the sample by the top. The volume of water injected by the top of the sample increased instantaneously after 125 days of hydration due to a manipulation of the burette connected to the hydration system; the water level was adjusted to the top of the cell. After 700 days of hydration, the volumes injected by the bottom and the top are 78.2 cm^3 and 128.2 cm^3 respectively. The total volume injected during the test is 206.4 cm^3. As it can be observed, the rate of increasing is still positive after 700 days of hydration. This suggests that the sample is not entirely saturated after 700 days of hydration.

The profiles of relative humidity at a time interval of 5 days are presented in Figure 12. At the beginning of the test, before hydration, different values are observed for every sensor (around 40% of relative humidity). This is because the initial suction is not homogeneous within the sample, thus the results depend on the local relative humidity. Then, while wetting, an instantaneously increase is observed at 31 mm and 111 mm, due to the proximity of the hydration front. The evolution of other sensors depends on the evolution of the hydration front. A total saturation (corresponding to a value of relative humidity of 100%) is observed after 40-

283 day hydration. However, it was observed that the rate of injected water is still positive after
284 700-day hydration. This means that the measured relative humidity value of 100% after 40 days
285 corresponds to the saturation of the large pores, and it does not represent the full saturation of
286 the sample.

287 5. Discussion

288 The anisotropy of swelling pressure observed in this investigation can be interpreted based on
289 two key features: (i) the dependence of the swelling pressure on the dry density of bentonite
290 and (ii) the initial heterogeneous distribution of the material. The swelling pressure evolution
291 of the sensor located at 100 mm (SP100) during the first 200 days (Figure 5) is due to the
292 presence of larger voids at this level, as it is observed in Figure 3. A peak is observed at the
293 beginning of the hydration process. This peak and consequent temporary drop corresponds to
294 the reorganization of the microstructure of the soil induced by the collapse of the larger voids,
295 so inter-pellet voids (Alonso et al., 2011; Gens et al., 2011). During hydration, pellets start
296 swelling and filling the larger voids between them. This kind of response can be associated to
297 the limit between two layers of pellets with powder of bentonite located in the inter-pellet voids,
298 as it can be observed in Figure 3 at 100 mm. The heterogeneous distribution of pellets and
299 powder within the sample plays an important role in the creation of these larger voids.

300 Figure 13 displays the evolution of swelling pressure with suction for sensors SP40, SP60, SP80
301 and SP100. As the positions of the RH sensors and SP sensors are not the same, an interpolation
302 of the evolution of the suction is carried out in order to estimate the suction at the same level as
303 the SP sensors. These calculations were not carried out for sensor SP20 as there is no RH
304 sensors between the bottom hydration front and SP20. For sensor SP100, from the initial state
305 (point A), a sudden increase of the swelling pressure is observed until a value of suction of 120
306 MPa. Then, a peak is observed (point B) due to the reorganization of the microstructure of the

307 soil induced by the collapse of the macro-pores (inter-pellets voids). Then, the swelling pressure
308 increases while wetting again until a constant value is reached (2.5 MPa) before saturation. It
309 is worth noting that the calculated suctions using RH measurements correspond to the local
310 macro structural suctions prevailing locally at the measured point. Unfortunately, the RH
311 sensors do not allow the measurement of the evolution of suction at the microstructural level
312 (micro-pores within pellets) which might experience a delay in hydration.

313 For other sensors (SP40, SP60 and SP80 in Figure 13) this behaviour is not observed. The shape
314 of the wetting path depends on the local density of the material, which depends on the
315 pellet/powder structural distribution at the corresponding position as well as the vicinity of the
316 hydration front. The increase rate of swelling pressure of sensor SP40 is negative at the
317 beginning of the test, which might be due to a reorganization of the macrostructure at this level.
318 The behaviour is different compared to sensor SP100 as no swelling is observed before the
319 collapse. The rate of increase of swelling pressure for SP40 is the lowest for the four sensors,
320 indicating that the material has a low dry density at this level. This response can be associated
321 to the limit of two layers of pellets with no grains of powder between the pellets. This
322 distribution can be observed in Figure 3 at 40 mm. For sensor SP60, a decrease in suction is
323 observed with no swelling before 50 MPa suction. It is believed that there is concentration of
324 bentonite powder grains in the vicinity of this sensor with no pellets (this kind of distribution
325 can be observed in Figure 3 between SP20 and SP60). Therefore, bentonite grains swell but no
326 pressure is recorded by the sensor until suction reaches 50 MPa due to its loose structure. For
327 sensor SP80, swelling pressure increases with a rate higher than SP60, but no collapse of the
328 macrostructure is observed. No constant value of swelling pressure is observed for both sensors
329 under a certain value of suction, as it was observed for sensor SP100, indicating that the
330 structure of the mixture is still changing at this state of the hydration process. After 700 days, a

331 common value of 4 MPa of swelling pressure is observed for radial sensors except SP100,
332 which value is slightly higher than 3 MPa.

333 Based on the initial average dry density of the mixture (1.49 Mg/m^3) and the relationships
334 between axial swelling pressure and dry density derived by Karnland et al. (2008) and Wang et
335 al. (2012), the final value of the axial swelling pressure is estimated. It ranges from 4.15 MPa
336 to 4.66 MPa. The lower measured value (2.5 MPa) is due to: (i) the material preparation
337 protocol, which results in a concentration of macrovoids at the top of the sample, where the
338 porous stone is in contact with some pellets without powder grains between them (Figure 3)
339 and (ii) the friction of the material with the cell while swelling (Saba et al., 2014), which is
340 transmitted to the force transduced. However, it is believed that the effect of friction is not as
341 significant as in the case of compacted bentonite/sand mixture. Therefore, the difference
342 between the axial and radial swelling pressure in this study is mainly due to the heterogeneity
343 of the material. Moreover, in the vicinity of the radial sensors, different pellets/powder
344 arrangements are clearly observed (Figure 3), which is due to the sample preparation process
345 in which the cell is filled by packets corresponding to one layer of pellets spread over the base
346 of the sample (see for instance Molinero Guerra et al., 2016). This lead to different responses
347 of the sensors. Note that other values of swelling pressure can be found in the literature for the
348 MX80 bentonite at 1.5 Mg/m^3 of dry density. Komine and Ogata (2004) found a value of 1.5
349 MPa at the mentioned suction, whereas Agus and Schanz (2008) found a value of 2.5 MPa.
350 These values differ from the relationships found by Karnland et al. (2008) and Wang et al.
351 (2012), showing a certain data scatter of the available data.

352 The total volume of injected water is 206.4 cm^3 after 700 days of hydration. However, taking
353 into account the dry density of the material, the theoretical injected volume when the mixture
354 is saturated should be 155 cm^3. This difference may be partially explained by the water density
355 changes (Jacinto et al., 2012; Marcial 2011). Based on the hypothesis that all water in the sample

356 is interlayer adsorbed water, a water density of 1.316 Mg/m^3 can be estimated from the
357 theoretical volume of injected water and the measured value. Marcial (2011) obtained a water
358 density of 1.02 Mg/m^3, 1.27 Mg/m^3 and 1.57 Mg/m^3 for a sample of compacted MX80 bentonite
359 at a dry density of 1.354 Mg/m^3, 1.691 Mg/m^3 and 1.952 Mg/m^3 respectively. It is worth noting
360 that the water in the interlayer zone of expansive clays has several features which are quite
361 different from those of free water. This increase in water density, which depends on the relative
362 humidity, could be partially associated with the predominant exchangeable cations in the clay,
363 and the difference in the interaction mechanisms between each cation and the interlayer water
364 (Jacinto et al., 2012). Possible water evaporation during the test should be considered as another
365 reason for this difference of water intake.

366 ## 6. Conclusions

367 In the context of the SEALEX project (IRSN), a small-scale test (1/10th) was performed in order
368 to investigate the HM behaviour of pellet/powder MX80 bentonite mixture. The swelling
369 pressure at different positions in the sample allowed better understanding the complex swelling
370 behaviour of this heterogeneous material.

371 The evolution of the radial swelling pressure for the different positions are due to the local
372 porosity of the material combined to the evolution of the hydration front. Local porosities
373 depend strongly on the initial heterogeneous distribution of pellets and powder within the
374 sample. A collapse of the material is observed at the sensor located at 100 mm due to the
375 presence of larger voids at this level, corresponding to the limit between two layers of pellets
376 with some bentonite powder grains between them. At 40 mm from the bottom, a collapse is
377 found at the beginning of the test with no previous swelling, due to the reorganization of the
378 macro structure at this level. This behaviour could be related to the limit between two layers of

pellets without powder grains between them. For the rest of the sensors, no collapse is observed because there are no macrovoids in the vicinity of the sensors.

The anisotropy observed between radial and axial swelling pressure is due to the presence of larger voids at the top of the sample, where the top pore stone contacts with some pellets without no powder grains between them, as well as the friction of the material with the cell while swelling. Note that the effect of friction could be much more significant in field scale. Moreover, it is believed that the sample is more compact radially than axially due to the fabrication process, which can greatly affect the pellet/powder distribution, and consequently the HM behaviour of the material.

The evolution of radial swelling pressure depends on the pellet/powder distribution. Different responses can be obtained even if the same protocol is followed. The final dry density profile is not entirely homogeneous at the end of test due to the initial heterogeneous distribution of porosities combined to the effect of friction and the non-saturation of the mixture.

During the saturation process, a difference was observed between the measured volume of injected water and that estimated by considering the total porosity. This difference is partially explained by changes in water density, as it was concluded by Jacinto et al. (2012) and Marcial (2011). The water density depends on the relative humidity, and it is associated with the predominant exchangeable cations in the clay, and the difference in the interaction mechanisms between each cation and the interlayer water. This dependence should be considered in the investigation on the performance of sealing plugs with bentonite-based materials.

References

Alonso, E.E., Vaunat, J. and Gens, A., 1999. Modelling the mechanical behaviour of expansive clays. Engineering Geology, 54(1-2), 173–183.

403 Alonso, E.E., Romero, E. and Hoffmann, C., 2011. Hydromechanical behaviour of compacted
404 granular expansive mixtures: experimental and constitutive study. Géotechnique 61(4),
405 329–344.

406 Agus, S.S. and Schanz, T., 2008. A method for predicting swelling pressure of compacted
407 bentonites. Acta Geotechnica 3(2), 125-137.

408 Börgesson, L., Karnland, O. and Johannesson, L. E., 1996. Modelling of the physical behaviour
409 of clay barriers close to water saturation. Engineering Geology 41(1-4), 127–144.

410 Dixon, D.A., Gray, M. N. and Graham, J., 1996. Swelling and hydraulic properties of bentonites
411 from Japan, Canada and the USA. Environmental Geotechnics 1, 43–48.

412 Garcia-Siñeriz, J.L., Villar, M. V., Rey, M. and Palacios, B., 2015. "Engineered barrier of
413 bentonite pellets and compacted blocks: State after reaching saturation," Engineering
414 Geology 192, 33–45.

415 Gens, A. and Alonso, E.E., 1992. A framework for behaviour of unsaturated expansive clays.
416 Canadian Geotechnical Journal 29, 1013–1032.

417 Gens, A., Vallejan, B., Sánchez, M., Imbert, C., Villar, M.V. and Van Geet, M., 2011. Hydro-
418 mechanical Behavior of a Heterogenous Compacted Soil: Experimental Observations and
419 Modelling. Géotechnique 61(5), 367-386.

420 Hoffmann, C., Alonso, E.E. and Romero, E., 2007. Hydro-mechanical behaviour of bentonite
421 pellet mixtures. Physics and Chemistry of the Earth 32(8-14), 832–849.

422 Imbert, C. and Villar, M.V., 2006. Hydro-mechanical response of a bentonite pellets/powder
423 mixture upon infiltration. Applied Clay Science 32(3-4), 197–209.

424 Jacinto, A.C., Villar, M.V. and Ledesma, A., 2012. Influence of water density on the water-
425 retention curve of expansive clays. Géotechnique 62(8), 657–667.

426 Josa, A., Alonso, E.E. and Gens, A., 1991. Discussion: A constitutive model for partially
427 saturated soils. Géotechnique 41(2), 273–275.

428 Karnland, O., Nilsson, U., Weber, H. and Wersin, P., 2008. Sealing ability of Wyoming
429 bentonite pellets foreseen as buffer material – laboratory results. Physics and Chemistry
430 of the Earth, Parts A/B/C 33, S472–S475.

431 Kaufhold, S., Baille, W., Schanz, T., and Dohrmann, R., 2015. About Differences of Swelling
432 Pressure - Dry Density Relations of Compacted Bentonites. Applied Clay Science 107,
433 52–61.

434 Komine, H., and Ogata, N., 2004. Predicting swelling characteristics of bentonites. Journal of
435 Geotechnical and Geoenvironmental Engineering 130, 818-829.

436 Lloret, A., Villar, M. V., Sánchez, M., Gens, A., Pintado, X. and Alonso, E. E., 2003. Me-
437 chanical behaviour of heavily compacted bentonite under high suction changes. Géotech-
438 nique 53(1), 27–40.

439 Marcial, D., 2011. A simple method to consider water density changes in the calcualtion of the
440 degree of saturation of swelling clays. In Unsaturated Soils: Proceedings of the Fitth
441 International Conference on Unsaturated Soils, Barcelona, Spain, 6-8 september 2010.
442 473-478.

443 Mokni, N. and Barnichon, J.D., 2016. Hydro-mechanical analysis of SEALEX *in situ* tests -
444 Impact of technological gaps on long term performance of repository seals. Engineering
445 Geology 205, 81–92.

446 Molinero-Guerra, A., Mokni, N., Delage, P., Cui, Y. J., Tang, A. M., Aimedieu, P., Bernier, F.
447 and Bornert, M., 2016. In-depth characterisation of a mixture composed of powder/pellets
448 MX80 bentonite. Applied Clay Science135, 538-546.

449 Saba, S., 2014. Hydro-mechanical behaviour of bentonite-sand mixture used as sealing
450 materials in radioactive waste disposal galleries. Université de Paris Est.

451 Saba, S., Cui, Y.J., Tang, A.M., and Barnichon, J.D., 2014. Investigation of the swelling
452 behaviour of compacted bentonite–sand mixture by mock-up tests. Canadian Geotechnical
453 Journal 51(12), 1399–1412.

454 Schanz, T. and Al-Badran, Y., 2014. Swelling pressure characteristics of compacted Chinese
455 Gaomiaozi bentonite GMZ01. Soils and Foundations 54(4), 748–759.

456 Van Geet, M., Volckaert, G. and Roels, S., 2005. The use of microfocus X-ray computed
457 tomography in characterising the hydration of a clay pellet/powder mixture. Applied Clay
458 Science 29(2), 73–87.

459 Villar, M. V., Gómez-Espina, R. and Guitiérrez-Nebot, L., 2012. Basal spacings of smectite in
460 compacted bentonite. Applied Clay Science 65–66, 95–105.

461 Villar, M.V., 2013. EB experiment. Contribution of CIEMAT to EB dismantling report. Phys-
462 ical state of the bentonite. EC Contract 249681 PEBS. Informe Técnico CIEMAT/DMA/
463 2G210/04/2013 (Madrid, 21 pp.).

464 Wang, Q., Tang, A.M., Cui, Y.J., Delage, P. and Gatmiri, B., 2012. Experimental study on the
465 swelling behaviour of bentonite/claystone mixture. Engineering Geology 124, 59–66.

466 Wang, Q., Tang, A.M., Cui, Y.J., Barnichon, J.D. and Ye, W.M., 2013. A comparative study
467 on the hydro-mechanical behaviour of compacted bentonite/sand plug based on labora-
468 tory and field infiltration tests. Engineering Geology 162, 79–87.

469

List of Tables

List of Figures

491 Table 1. Chemical composition of the synthetic water

Components	$NaHCO_3$	Na_2SO_4	NaCl	KCl	$CaCl_2$ $2H_2O$	$MgCl_2O6H_2O$	$SrCl_26H_2O$
Mass (g) per litre of solution	0.28	2.216	0.615	0.075	1.082	1.356	0.053

492

493

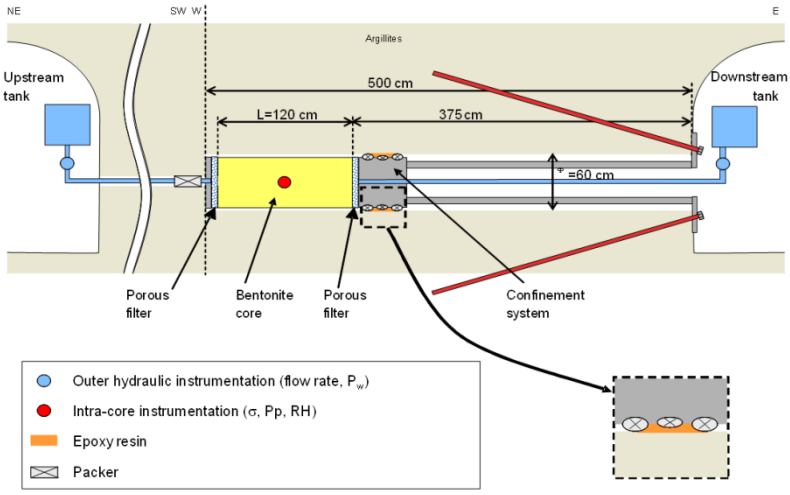

Figure 1. Layout of the SEALEX *in situ* tests (after Mokni et al., 2016).

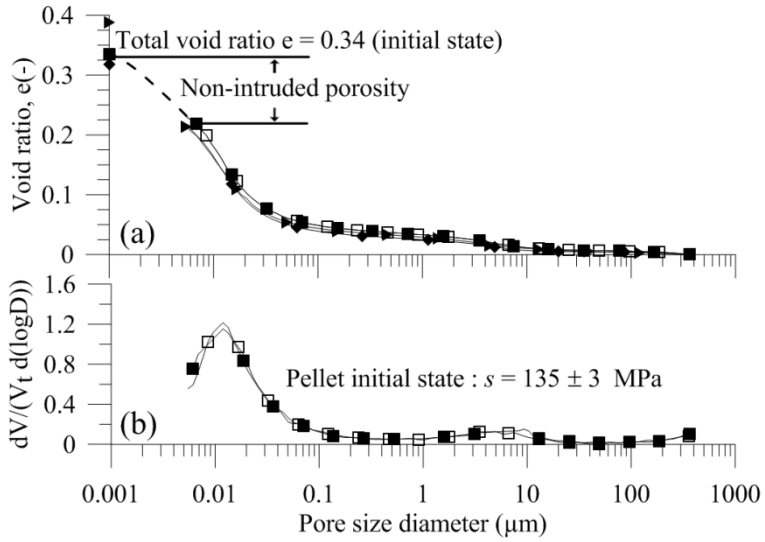

Figure 2. MIP tests results for a pellet of bentonite at its initial state.

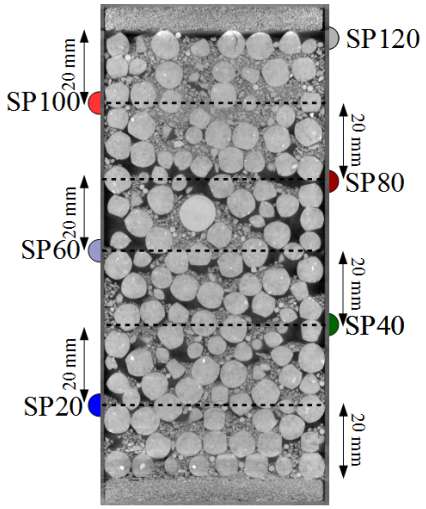

Figure 3. Vertical section of the investigated pellet/powder bentonite mixture obtained by µ-CT observations. Resolution: 50 µm/voxel.

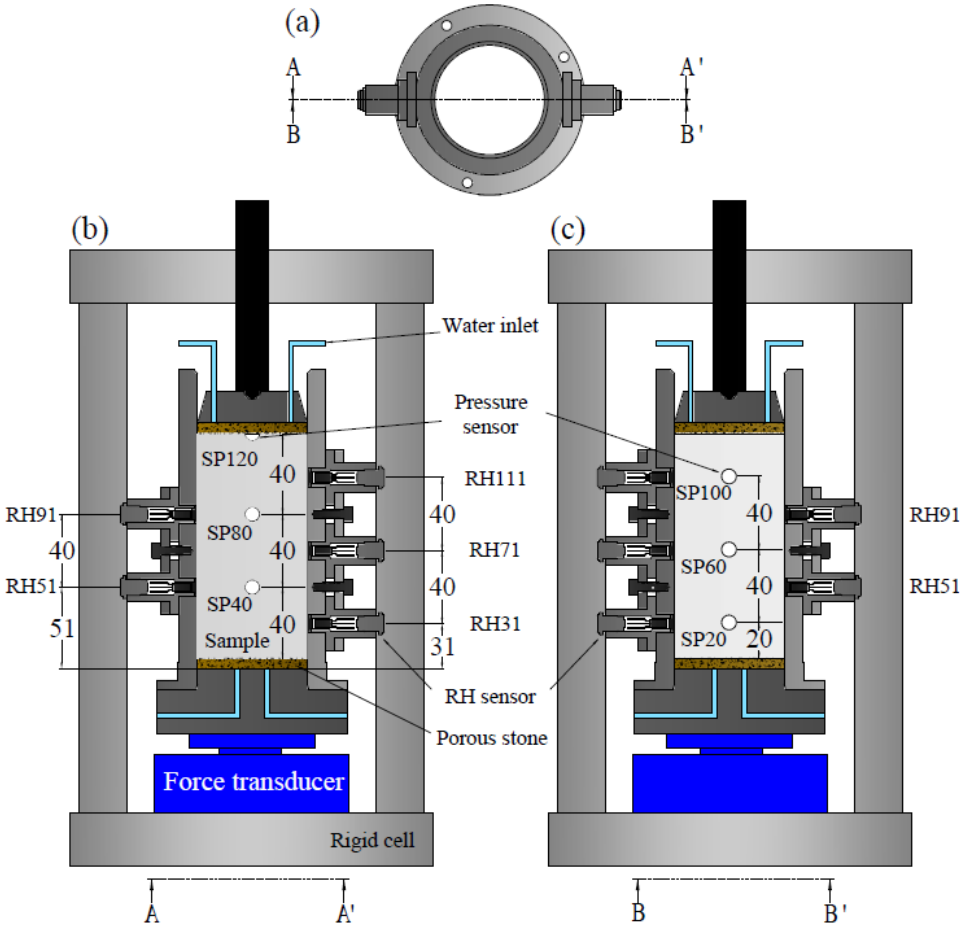

Figure 4. Layout of the mock-up test cell (a) seen from above; (b) section A-A'; (c) section B-B' (dimensions in mm).

509

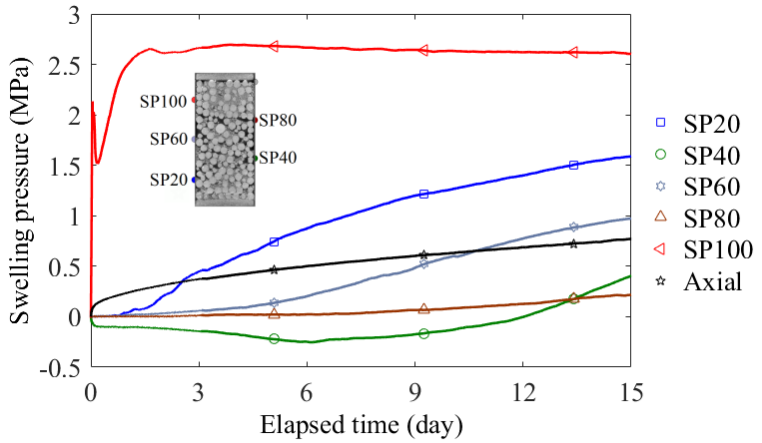

510

511 Figure 5. Evolution of the swelling pressure with time after 15 days of hydration.

512

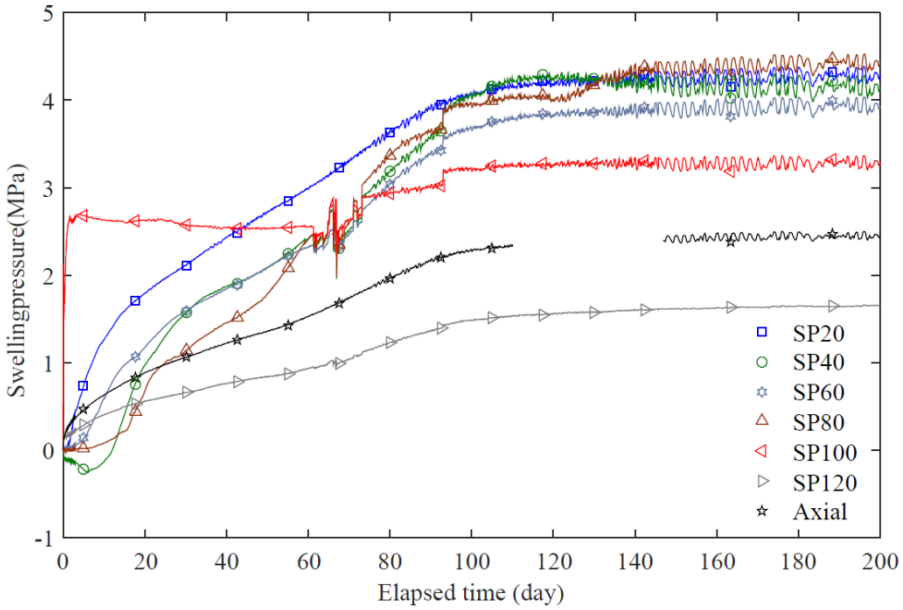

513

514 Figure 6. Evolution of the swelling pressure with time after 200 days of hydration.

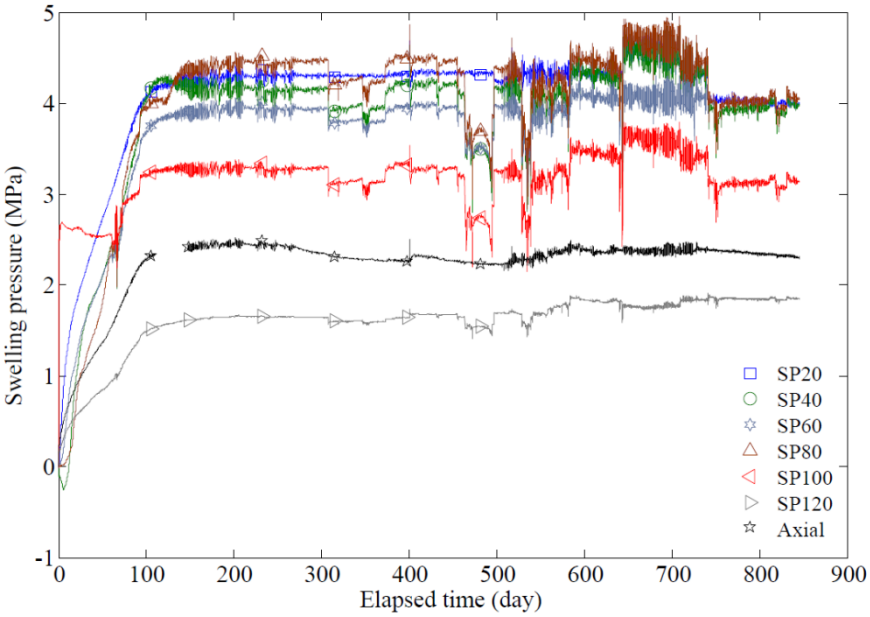

Figure 7. Evolution of the swelling pressure with time after 845 days of hydration.

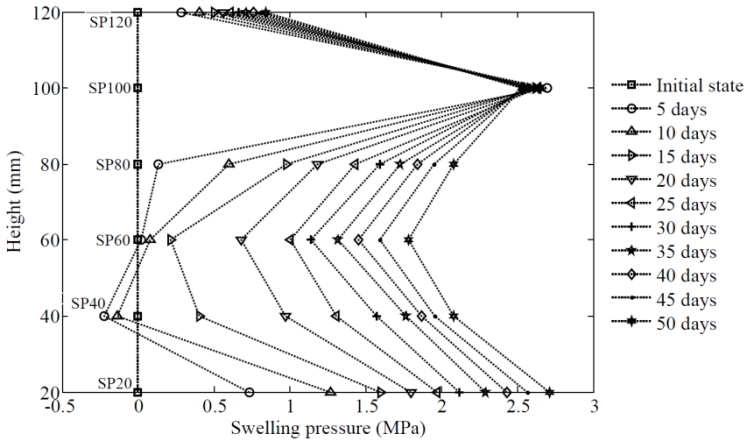

Figure 8. Swelling pressure profiles at different times (every 5 days).

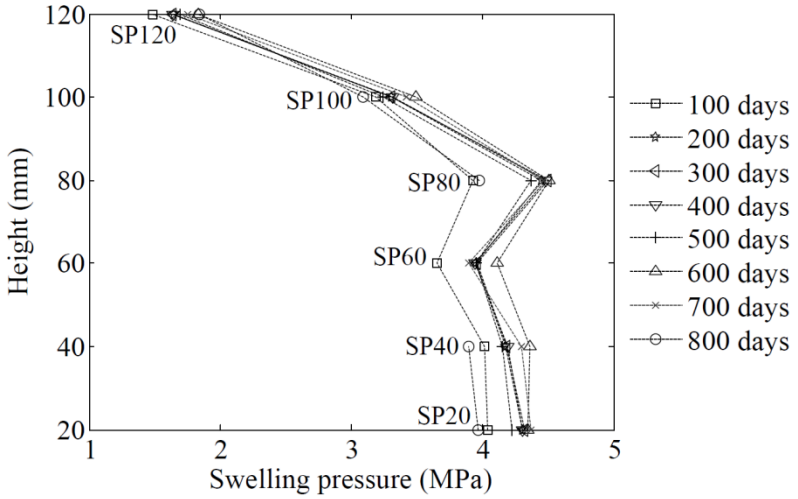

Figure 9. Swelling pressure profiles at different times (every 100 days).

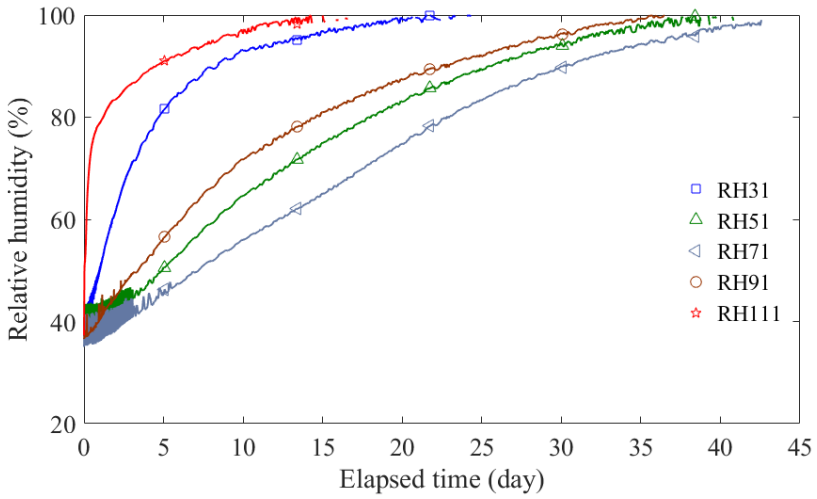

Figure 10. Evolution of the relative humidity with time.

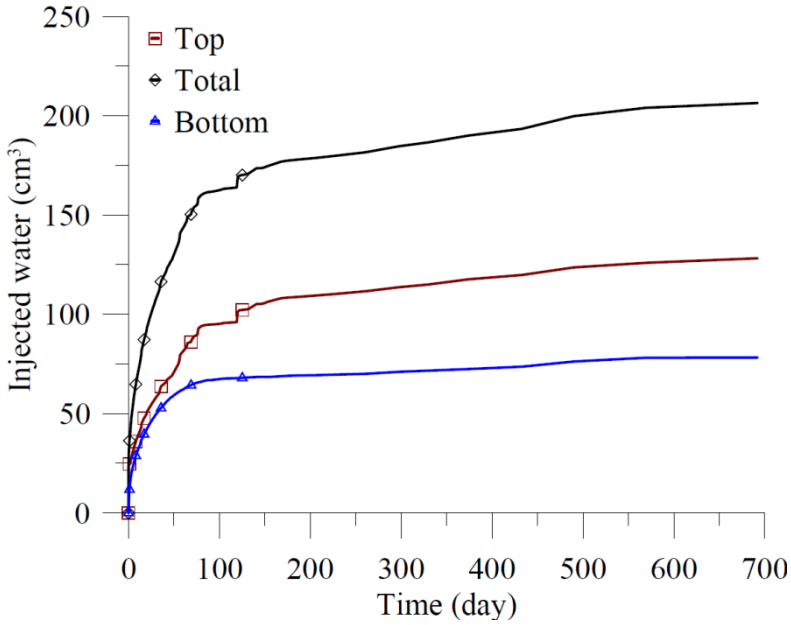

Figure 11. Evolution of the injected water with time during hydration.

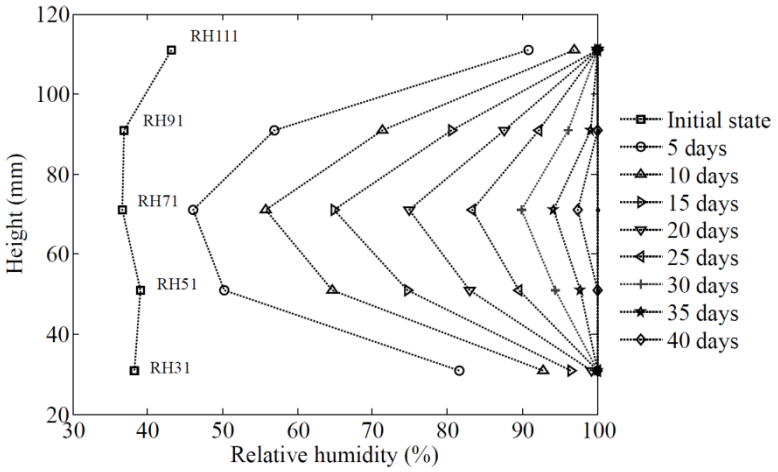

528

529 Figure 12. Relative humidity profiles at different times (every 5 days).

530

531

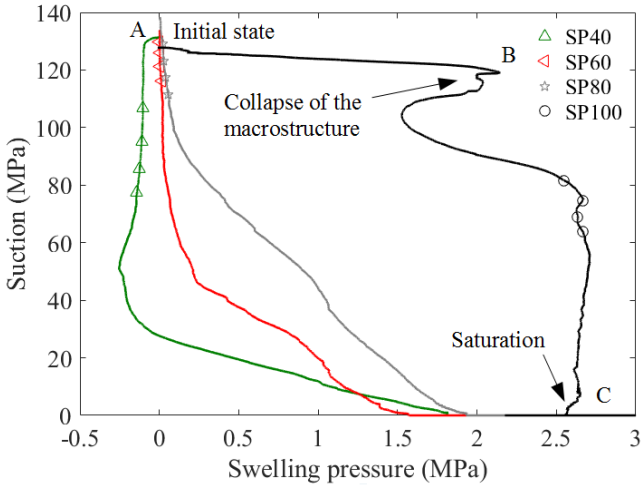

532

533 Figure 13. Suction versus swelling pressure at different positions.

534

535

536

537